Coexistence of Crew-Cut and Starlike Spherical Micelles Composed of Copolymers with an Annealed Polyelectrolyte Block

Y. Lauw,* F. A. M. Leermakers, and M. A. Cohen Stuart

Laboratory of Physical Chemistry and Colloid Science, Wageningen University, Dreijenplein 6, Wageningen 6700 EK, The Netherlands

O. V. Borisov[†,‡] and E. B. Zhulina[†]

Institute of Macromolecular Compounds of the Russian Academy of Sciences, 199004, St. Petersburg, Russia, and DRFMC/SI3M CEA-Grenoble, 38000 Grenoble, France, and LPCP, UMR 5067 CNRS/ UPPA 2, av. President Angot, 64000 Pau, France

Received January 23, 2006; Revised Manuscript Received March 21, 2006

ABSTRACT: The self-assembly of block copolymer A_mB_n into spherical micelles is analyzed using a numerical self-consistent-field theory. A is the hydrophilic annealed polyacid and B the hydrophobic part. The degree of polymerization for the polar moiety is fixed ($m = 100$), whereas that of the tail is varied ($n = 100$, 200, and 300). The charge in the annealed A block depends on both the pH and the added 1:1 electrolyte concentration φ_s. Beyond the cmc, the diblock copolymers form either low aggregation number starlike or large aggregation number crew-cut micelles. A nonmonotonic behavior of the micellar properties as a function of φ_s for fixed pH is found. For starlike micelles, the scaling of the aggregation number N_{agg} with φ_s is in fair agreement with analytical predictions, i.e., $N_{agg} \sim \varphi_s^{0.7-0.9}$. For the core radius, we find that $R_{core} \sim \varphi_s^{0.24-0.3}$, and for the corona thickness $T_{corona} \sim \varphi_s^{-0.08}$. For crew-cut micelles, the scaling exponents deviate significantly from analytical predictions. Upon increasing pH, a smooth transition from crew-cut to starlike micelles happens at high φ_s. Interestingly, a coexistence between these two different micellar sizes is possible for relatively low values of φ_s in a narrow pH range. The corresponding thermodynamics, phase diagram, and various structural properties are presented.

I. Introduction

The study of the self-assembly of amphiphiles into association colloids has received ample attention in the literature due to its many important applications in various fields, such as formulation science, surface chemistry (wetting), pharmacy (drug delivery), and environmental sciences (soil remediation).[1−4] Analogous to low molecular weight surfactants, in a selective solvent block copolymers self-assemble into mesoscopic objects. Beyond a particular concentration, which is known as critical micellization concentration (cmc), the polymeric surfactants form so-called micelles. In aqueous solvents, a micelle consists of a dense hydrophobic core and a strongly hydrated corona. Polymeric systems have an intrinsic advantage over low molecular weight surfactants as the chain length of each block can be widely varied without loosing thermodynamic stability of the micelles. A large degree of freedom of block lengths give a flexibility to adjust the copolymers to a particular application. It is obviously more convenient when the copolymer self-assembly is responsive to simple physicochemical conditions without the need to adjust the block lengths.

There are strong indications that micelles consisting of block copolymers with both a hydrophobic and an annealed polyelectrolyte block have remarkable responsive structural properties. Borisov and Zhulina published an extensive theoretical study for the self-assembly of this type of block copolymers in an aqueous electrolyte solution.[5,6] Their major findings are briefly reviewed in this article.

From a scaling point of view, two types of spherical micelles were defined: the so-called starlike (or hairy) and crew-cut micelles. These two micellar shapes are defined on the basis of the relative size of their core radius with respect to the corona thickness. A micelle has a starlike shape when the thickness of the corona exceeds the radius of the core. The micelle has a crew-cut shape when the radius of the core is larger than the thickness of its corona. An illustration of these two cases is presented in Figure 1. These different micellar morphologies are experimentally observed for diblock copolymers which usually consist of a polystyrene hydrophobic block and a carboxylated hydrophilic part.[7−13]

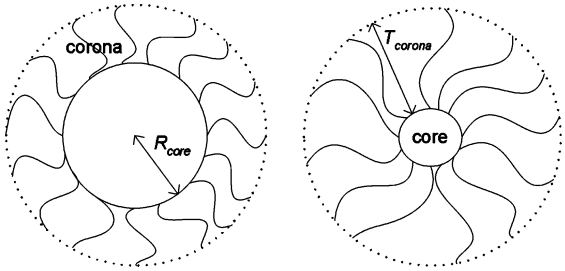

Figure 1. Schematic illustration of a crew-cut (CC) micelle (left) and a starlike (SL) micelle (right). The core mainly consists of hydrophobic chain parts and parametrized by R_{core}, the radius of the core. The corona is composed of polyacid segments, and T_{corona} refers to the corona thickness.

The corona mainly consists of weak polyacids. For a fixed value of the (intrinsic) dissociation constant pK_a of the polyelectrolyte block, the degree of dissociation depends naturally on the pH. Within the micelle, the charged groups induce a local electrostatic potential Ψ. This potential counteracts further dissociation of the acid groups. Small, indifferent ions screen the charges and thus damp the electrostatic potential. As a result, the dissociation also becomes a function of the salt concentration

[†] Russian Academy of Sciences and DRFMC/SI3M CEA-Grenoble.
[‡] LPCP.

10.1021/ma060163t CCC: $33.50
Published on Web 04/15/2006

φ_s (in this article, a dimensionless volume fraction of salt is used). In equilibrium, the charge in the corona is, to a good approximation, compensated by counterions (Donnan equilibrium).

For micelles with a liquidlike micellar core, Borisov and Zhulina predicted that the pH and φ_s dependences of the degree of dissociation have nontrivial effects on the micellization.[5,6] In particular, when pH $\approx$ pK_a, various micellar properties of the system, such as the size and aggregation number, vary nonmonotonically with the electrolyte concentration.[6−15] At pH $\ll$ pK_a or pH $\gg$ pK_a, the micellar behavior changes monotonically with varying electrolyte concentration.

The analytical model,[5,6] which presumed a boxlike structure of the corona, predicted that the presence of the annealed polyelectrolyte block may lead to an abrupt transition in micellar size. It was also predicted that a starlike form can coexist with a crew-cut structure, while the intermediate sizes are forbidden.[6] This is quite remarkable since the predicted transition does not involve a topological change (both micellar entities have a spherical geometry). These theoretical predictions form the guidelines and the motivation for a more rigorous and realistic modeling of these micelles by using a numerical SCF model.

The self-assembly of diblock copolymers with an annealed polyelectrolyte block is analyzed in the present paper by applying the self-consistent-field (SCF) theory, using the numerical scheme of Scheutjens and Fleer (SF-SCF).[16,17] The SF-SCF theory combines a first-order Markov approximation for the chain statistics with a local mean-field approximation. For a fixed preset geometry, it assumes a homogeneity of the density of molecular components in planes and allows for gradients in the normal direction. The SCF method has been used before to study the self-assembly of uncharged block copolymers in a selective solvent.[18] The Poisson−Boltzmann equation is used to incorporate charged components. The self-assembly of ionic surfactants has been studied by, e.g., Bohmer et al., who applied the SF-SCF scheme for both bulk micellization and adsorption phenomena,[19,20] and by Meijer et al.,[21−24] Claessens et al.,[25] and Rabinovich and Leermakers et al.,[26,27] who studied phospholipid bilayers. Within the SCF model, annealed charges are treated in terms of a multiple-state model.[28] The adsorption of block copolymers with an annealed polyelectrolyte block, or brushes made from these chains, has already been considered.[29] However, the study of micellar formation of block copolymers with an annealed polyelectrolyte block has not yet been attempted with the SF-SCF method. Below, we show that the analytical predictions of Zhulina and Borisov[5,6] are consistent with our numerical calculations and that it is indeed possible that two different micellar sizes coexist. Interestingly, micellar coexistence is consistent with the presence of a first-order-like phase transition.

At this stage, it is important to recall the notion of the thermodynamic limit when dealing with phase transitions. In particular, for a system that features a first-order phase transition, one typically will have two distinct macroscopic states of the system, i.e., gas−liquid or liquid−liquid phase separation. There is a well-defined set of chemical potentials at which the coexistence is possible, and the free energy landscape features two local minima separated by an infinitely high maximum. The composition of coexisting phases is given by the so-called binodal. When the overall composition changes, only the volumes of the two coexisting phases change and not their compositions (their chemical potentials are fixed). Only in the single-phase regions of the phase diagram, the chemical potentials become a function of the average composition. It is known that for systems in which the coexisting phases are not macroscopic in size a true first-order phase transition cannot occur. One of the key examples of a system that suffers from finite-size effects is the self-assembly of surfactants (copolymers) into micelles. For micellar systems, phase transition-like phenomena can be envisioned, although there may be many intricacies. To illustrate this, it is relevant to discuss how free copolymers exist in equilibrium with small micelles.

It is obvious that the volume of a single micelle remains microscopic; i.e., the length scale remains in the order of the copolymer size. Again, one important consequence of this is that the micellar formation cannot proceed through a first-order phase transition. Nevertheless, very often one can identify a critical micellization concentration (cmc) which refers to a binodal-like phenomenon connected to a first-order phase transition. However, for the micellar system, it is not correct that the chemical potential of the copolymer remains fixed when the total number of micelles is increased (by increasing the overall copolymer concentration above the cmc). In fact, it can be shown that the chemical potential of the surfactants (copolymers) increases slightly with increasing micelle concentration. As the chemical potential increases, there must be a concomitant growth of the micellar size which may be significant. For a sufficiently high aggregation number, the change in chemical potential is very small (the chemical potential is fixed in the first order), and the growth of micellar size with copolymer concentration remains limited. Therefore, one can view micellar formation as a first-order-like phase transition. As it will be discussed below, all of these aspects are incorporated in the thermodynamics of small systems and retrieved in all the details in the SCF modeling of micellar formation.

As previously mentioned, the charged annealed block copolymer system leads to the possible presence of two distinct kinds of stable micelles that coexist at the same chemical potentials. As intermediate micelle sizes are not stable, we are confronted with an interesting type of phase coexistence, which is again reminiscent of a first-order-like phase transition. Apparently, the free energy landscape must feature two local minima separated by a maximum with a finite height. This leads to the presence of finite size effects. For example, we should anticipate that it is possible to change the ratio between the numbers of the two types of micelle simply by changing the amount of copolymers in the system. However, such change cannot occur at fixed chemical potentials. As a natural consequence, the two micellar species will necessarily be responsive to changes of the chemical potentials. The thermodynamics of small systems that is compatible with two distinct micellar species will be discussed below in some depth. Furthermore, in the discussion, we will come back to the physics of phase coexistence in small systems.

The outline of the remainder of this article is as follows: We first describe the application of thermodynamics of small system to the analysis of the SF-SCF calculation. This is followed by the review on the statistical modeling, in particular, the SCF theory for an inhomogeneous system of copolymers that is combined with a summary of all input model parameters. The article is closed by the description of the results and conclusions.

II. Thermodynamics of Small System

The thermodynamical background of self-assembly has a solid foundation in the thermodynamics of small system initiated by Hill.[30] It was elaborated further for the case of surfactant micellization by Hall and Pethica.[31] The SF-SCF model is ideally suited to give the (statistical) thermodynamical framework that implements the small system analysis. This method

has been used previously for surfactant (copolymer) systems. Here, we review the important steps and apply the method to deal with the coexistence of crew-cut and starlike micelles.

In the classical thermodynamics, according to Gibbs,[32] in a macroscopic system consisting of c components, the change of internal energy dU due to the change of entropy dS, volume of the system dV, and the total number of molecules of the ith component dN_i, at temperature T, pressure p, and chemical potential of all components μ_i, is given by

$$\mathrm{d}U = T\,\mathrm{d}S - p\,\mathrm{d}V + \sum_i^c \mu_i\,\mathrm{d}N_i \tag{1}$$

In the case of micellization, this expression is extended by introducing two conjugated quantities, i.e., the subdivision potential $\mathcal{E}$ and the number of micelles $\mathcal{N}$,[30,31] such that

$$\mathrm{d}U = T\,\mathrm{d}S - p\,\mathrm{d}V + \sum_i^c \mu_i\,\mathrm{d}N_i + \mathcal{E}\mathrm{d}\mathcal{N} \tag{2}$$

Therefore, the change of the Helmholtz energy dF, where $F = U - TS$, can be expressed as

$$\mathrm{d}F = -S\,\mathrm{d}T - p\,\mathrm{d}V + \sum_i^c \mu_i\,\mathrm{d}N_i + \mathcal{E}\mathrm{d}\mathcal{N} \tag{3}$$

where the equilibrium and the stability conditions lead to two constraints:

$$\left.\frac{\partial F}{\partial \mathcal{N}}\right|_{T,V,\{N_i\}} = \mathcal{E} = 0 \tag{4}$$

$$\left.\frac{\partial^2 F}{\partial \mathcal{N}^2}\right|_{T,V,\{N_i\}} = \left.\frac{\partial \mathcal{E}}{\partial \mathcal{N}}\right|_{T,V,\{N_i\}} > 0 \tag{5}$$

Equation 4 ensures that at equilibrium the macroscopic thermodynamics for a homogeneous phase, as expressed in eq 1, is conserved. Equation 5 assures the stability of the micellization. Furthermore, under isothermic conditions, based on eq 3, one obtains

$$F = -pV + \sum_i^c \mu_i N_i + \mathcal{E}\mathcal{N} \tag{6}$$

or equivalently

$$F + pV - \sum_i^c \mu_i N_i = \mathcal{E}\mathcal{N} \tag{7}$$

The complete subdivision potential $\mathcal{E}$ cannot be computed by SCF type of modeling. The reason is that in the numerical procedure one considers a single micelle in the center of the coordinate system. Instead, the grand potential per micelle Ω is obtained and interpreted as the translationally restricted $\mathcal{E}$. Therefore, an extra entropic term S_{extra}, which is coupled to degrees of freedom at the level of the whole micellar object and that is ignored by the SCF method, has to be added to regain the complete subdivision potential

$$\Omega - TS_{\mathrm{extra}} = \mathcal{E} \tag{8}$$

As already referred to in the Introduction, in the SCF system (one micelle is in the center of the coordinate system), equivalent to eq 5, the relevant stability constraint is reformulated as

$$\left.\frac{\partial \Omega}{\partial \mathcal{N}}\right|_{T,V,\{N_i\}} > 0 \tag{9}$$

Since in a closed system with constant number of surfactants (copolymers) the number of micelles $\mathcal{N}$ is reduced upon increasing aggregation number N_{agg}, the stability condition can be rewritten as

$$\left.\frac{\partial \Omega}{\partial N_{\mathrm{agg}}}\right|_{T,V,\{N_i\}} < 0 \tag{10}$$

If stable monodisperse micelles exist for a particular chemical potential of copolymers, the extra entropic term S_{extra} is just the translational entropy S_{trans} of a micelle, i.e., $S_{\mathrm{trans}} \simeq -k_{\mathrm{B}} \ln \varphi_{\mathrm{m}}$, where φ_{m} is the volume fraction occupied by a micelle. As the system is macroscopically homogeneous and each small system has a single micelle, the volume fraction of the micelle is given by the ratio of the intrinsic volume of the micelle v_{m} and the volume of the small system $v = V/\mathcal{N}$. The intrinsic volume of the micelle can be estimated by

$$v_{\mathrm{m}} \simeq \theta_{\mathrm{p}}^{\mathrm{exc}} a^3 \tag{11}$$

where $\theta_{\mathrm{p}}^{\mathrm{exc}}$ is the total excess number of copolymer segments in the micelle, i.e., the aggregation number N_{agg} multiplied by total number of segments of each copolymer. The parameter a is the characteristic size of a lattice site where one segment is located. Therefore, a^3 is the unit volume of each segment (further discussion about the discretization and numerical scheme can be found in the next section). By using expression 11, the micellar volume fraction can be written as

$$\varphi_{\mathrm{m}} = \frac{\theta_{\mathrm{p}}^{\mathrm{exc}}}{v} a^3 = \frac{\theta_{\mathrm{p}}^{\mathrm{exc}} \mathcal{N}}{V} a^3 \tag{12}$$

Obviously, the Ansatz $S_{\mathrm{trans}} \simeq -k_{\mathrm{B}} \ln \varphi_{\mathrm{m}}$ only applies when the micelle is in a very dilute solution such that there are no steric and electrostatic interactions between micelles (for the case of ionic micelle). In a dilute solution and at equilibrium, the micelle volume fraction φ_{m} is thus directly related to the grand potential

$$\varphi_{\mathrm{m}} = \mathrm{e}^{-\Omega/k_{\mathrm{B}}T} \tag{13}$$

Note that in the SCF model one obtains the most likely micellar size and fluctuations around this size are ignored. In eq 13, the entropy associated with the fluctuations in size is not included, whereas it should be accounted for in a more complete model.[33] Here, we restrict ourselves to the first-order effects.

In the SCF model, there is only one micelle in the system which is in equilibrium with a dilute copolymer solution. Nevertheless, from the SCF model, it is possible to understand how different micelles can coexist. This happens when for various micelles both equilibrium and stability constraints are fulfilled at a fixed set of intensive variables $\{\mu_i\}$. In this case, it is believed that S_{extra} contains both translational and mixing entropy contributions.

If there are, for example, two stable micelles that differ in size, then there are two restricted grand potentials Ω_1 and Ω_2. Let the volume V contains $\mathcal{N}_1$ (small) micelles of type 1 and $\mathcal{N}_2$ (large) micelles of type 2. The micelle of type 1 occupies a small system with volume v_1, and the micelle of type 2 occupies a different small system with volume v_2. These micelles are characterized by the same micellar volume fraction φ_{m} (cf. eq 12)

$$\varphi_m = \frac{\theta_p^{exc_1}\mathcal{N}_1 + \theta_p^{exc_2}\mathcal{N}_2}{V} a^3 \quad (14)$$

where $\theta_p^{exc_1}$ and $\theta_p^{exc_2}$ are the total excess numbers of copolymer segments in the micelle 1 and 2, respectively. All the micelles exist in a single ($\mathcal{N}_1$, $\mathcal{N}_2$, v_1, v_2, T) system in which the total volume of the system $V = \mathcal{N}_1 v_1 + \mathcal{N}_2 v_2$. The whole system consists of $\mathcal{N}_1 + \mathcal{N}_2$ small systems; each contains either a large or a small micelle. Therefore, the expression of the grand potential of the total system is

$$\Omega = \mathcal{N}_1\Omega_1 + \mathcal{N}_2\Omega_2 \quad (15)$$

In equilibrium, there are two contributions to the extra entropy S_{extra} that should be added. These are the translational entropy of micelles S_{trans} within their small system volumes v_1 and v_2, i.e., $S_{trans} \simeq -k_B(\mathcal{N}_1 \ln \varphi_m + \mathcal{N}_2 \ln \varphi_m)$, and the mixing entropy of two different types of micelle, $S_{mix} \simeq -k_B(\mathcal{N}_1 \ln X_1 + \mathcal{N}_2 \ln X_2)$. Here, X_1 and X_2 are the mole fractions of small systems of type 1 and 2 in the system

$$X_1 = \frac{\mathcal{N}_1}{\mathcal{N}_1 + \mathcal{N}_2} \quad (16)$$

$$X_2 = \frac{\mathcal{N}_2}{\mathcal{N}_1 + \mathcal{N}_2} \quad (17)$$

Obviously, $X_1 + X_2 = 1$, which indeed expresses the volume conservation. The use of the same micellar volume fraction φ_m in the translational entropy S_{trans} for both micellar sizes implies a macroscopically homogeneous distribution of copolymers in the small systems 1 and 2 since both small systems contain the same overall amount of copolymers. The mixing entropy S_{mix} accounts for the number of ways to distribute $\mathcal{N}_1$ micelles of type 1 and $\mathcal{N}_2$ micelles of type 2 over the whole system. By using the above expressions of translational and mixing entropies, the grand potential Ω_i of the small system with micelle of type i is

$$\Omega_i = T(S_{trans_i} + S_{mix_i}) = -k_B T(\ln \varphi_m + \ln X_i) \quad (18)$$

where $i = 1, 2$. Equivalently

$$X_i \varphi_m = e^{-\Omega_i/k_B T} \quad (19)$$

It has to be noted that the variables φ_m, X_i, and Ω_i depend on the total copolymer concentration φ_p, and from the mass conservation, one finds that

$$\varphi_p = \varphi_p^b + X_1\varphi_m + X_2\varphi_m \quad (20)$$

By substituting eq 19 into the expression 20, one obtains

$$\varphi_p = \varphi_p^b + e^{-\Omega_1/k_B T} + e^{-\Omega_2/k_B T} \quad (21)$$

expressing that for a given coexistence of two micellar sizes the copolymers in the system can be found either in the bulk as free molecules (first term on the rhs), in small micelles (second term), or in large micelles (last term).

III. Statistical Modeling

From the above description, it is clear that it is necessary to generate the grand potential Ω for micelles composed of a given number of copolymers as well as to predict its structure as a function of the copolymer concentration and other physicochemical characteristics of the system. The statistical thermodynamics provides the machinery for a given molecular model. To illustrate this point, it is of use to discuss briefly how the statistical thermodynamics is implemented in the analytical framework typically used for polymeric micelles.[5,6]

We consider a solution with volume V that contains N block copolymer molecules. We assume that there are N_0 block copolymers are free as unimers and that $N - N_0 = N_{agg}\mathcal{N}$ monomers are in micelles, where $\mathcal{N}$ is the total number of micelles (typically in the polymer literature N_{agg} is denoted as p). In a canonical ensemble, the Helmholtz energy $F(N,V,T)$ is the characteristic function. Assuming the dilute solution, one can model the micellar system as an ideal gas of particles

$$\frac{F}{k_B T} = N_{agg}\mathcal{N}\frac{F_p}{k_B T} + \mathcal{N}\ln\left(\frac{\mathcal{N}}{eV}\right) + (N - N_{agg}\mathcal{N})\frac{F_0}{k_B T} + (N - N_{agg}\mathcal{N})\ln\left(\frac{N - N_{agg}\mathcal{N}}{eV}\right) \quad (22)$$

Here, the first term is the free energy of the micelle (F_p is the free energy per monomer in micelles), and the second term is the translational entropy of the micelles. In a slightly better approximation, one should also account for the volume of the micelle to enumerate the micellar translational entropy (see also the previous section, cf. eq 12). The third term is the free energy of the unimers (F_0 is the free energy per unimer), whereas the final term is the translational entropy of the unimers. In the dilute solution the solvent concentration is considered to be high and constant such that the free energy contribution is safely neglected.

The free energy is then optimized both with respect to the number of micelles $\mathcal{N}$ and the aggregation number N_{agg} that leads to

$$F_p + N_{agg}\frac{\partial F_p}{\partial N_{agg}} - F_0 - k_B T \ln\left[\frac{N - N_{agg}\mathcal{N}}{V}\right] = 0 \quad (23)$$

$$F_p + \frac{k_B T}{N_{agg}}\ln\left(\frac{\mathcal{N}}{V}\right) - F_0 - k_B T \ln\left[\frac{N - N_{agg}\mathcal{N}}{V}\right] = 0 \quad (24)$$

The grand potential of the translationally restricted micelle is given by

$$\Omega = N_{agg}(F_p - \mu_p) \quad (25)$$

where the chemical potential μ_p of the free polymer chains is given by $\mu_p = F_0 + k_B T \ln[(N - N_{agg}\mathcal{N})/V]$. By applying eq 23, the partial derivative of the grand potential Ω with respect to N_{agg} leads to the Gibbs−Duhem relation

$$\frac{\partial\Omega}{\partial N_{agg}} = -N_{agg}\frac{\partial\mu_p}{\partial N_{agg}} < 0 \quad (26)$$

since $\partial\mu_p/\partial N_{agg} > 0$ for stable micelles. Equation 26 is thus consistent with eq 10. By introducing the mole fraction of micelles as $x_m = \mathcal{N}/V$, eq 24 reduces to

$$x_m = e^{-\Omega/k_B T} \quad (27)$$

which is equivalent to eq 13 when the volume of the micelle is ignored in the translational entropy of the micelle. We note that the molecular modeling is easily extended to account for different populations of micelles.

To evaluate the relevant free energies F_p and F_0, typically further approximations about the structure of the micelle are needed, e.g., with respect to the geometry of the micelles, the sharpness of the core−corona interface, the penetration of the solvent in the micelle, etc. For such details we refer to the corresponding articles.[5,6]

At some stage of the procedure, it becomes useful to choose a typical micelle out of the range of stable micelles. In many cases, the Ansatz is to ignore the translational entropy of the micelles (second term in eq 22). This directly leads to the equilibrium condition at which $\Omega = 0$. In other words, instead of a range of micelle sizes that are stable, one focuses on the micelle with vanishing grand potential value. This choice allows a systematic study toward the scaling relations in polymeric micelles. Of course, one can do the same in the numerical SCF model. However, we choose below to remain closer to experimental system and select quite arbitrarily the micelle with $\Omega = 10k_BT$ as a representative micelle that can be observed experimentally in (dilute) micellar solutions. It is easily seen that the small difference in choice for Ω does not disrupt the comparison between the analytical and numerical approaches.

A. Self-Consistent-Field Theory and Model Parameters. In the analytical models, approximations are needed to compute F_p and F_0 in order to evaluate Ω. Within the self-consistent-field approach, it is possible to obtain the (mean-field) partition function accurately without the need to put constraints onto the molecules. From the partition function and the corresponding characteristic function, the grand potential can be derived without further approximations. The main approximation in mean-field partition functions is that the binary distribution function between pairs of particles or atoms, which is needed to account the binary interactions, is replaced by a singlet distribution function for a particle (atom) in a self-consistent (external) potential u. Particularly in densely packed systems (as is the case in micellar solutions), the difference between the *actual* surroundings of a molecule does not differ too much from the *average* one. As a result, such a mean-field approach is reasonably accurate. In the following, we introduce the molecular model and give the essential background information on the SCF theory used for the micellization of diblock copolymers.

It is essential to mention that in any SCF method the symmetry of the system must be specified and fixed during the calculations. Here we use a discrete SCF model imposing a spherical geometry. This means that we will only focus on spherical micelles. We use the discretization scheme of Scheutjens and Fleer (SF-SCF) where the molecules are assumed to be composed of segments. These segments fit on lattice sites,[16,17] and lattice sites are arranged in layers which are numbered $r = 0, ..., M$. The number of lattice sites $L(r)$ in each layer grows quadratically with the layer number r, i.e., $L(r) \sim r^2$, where $r = 0$ is the center of the coordinate system that will coincide with the center of mass of the micelle, and $r = M$ is the last lattice layer in the system. We choose $M = 150$, which is a sufficient number such that the micelles are isolated; i.e., it exceeds significantly the Debye length. There is one characteristic length $a = 0.3$ nm which is associated with the size of a lattice site. It is used below to normalize all other linear lengths. Since the numerical discretization of the SF-SCF model requires us to use dimensionless concentrations (volume fractions), thus for the monomeric components, one has to multiply volume fraction by 55.4 to obtain concentration in mol/L (the conversion value of water, modeled as a monomer, with unity bulk volume fraction). As an example, the volume fraction of salt $\varphi_s = 10^{-5}$ is equal to the experimental salt concentration 5.5×10^{-4} M. Furthermore, in this lattice system, the a priori step probability to move inward, outward, or to remain in the layer depends on the coordinate r. It is assumed that these step probabilities go to $^1/_3$ in the limit of large r. These probabilities are used to account for the geometric-dependent local averages.[34]

The linear sequence of segments specifies the chain molecules. Here we use copolymers that consists of hydrophobic block B with length n and a polyacid block A with degree of polymerization m, i.e., A_mB_n, with the total degree of polymerization $\tilde{N} = m + n$. Three types of copolymers, $A_{100}B_{100}$, $A_{100}B_{200}$, and $A_{100}B_{300}$, are used. In addition, there is a 1:1 electrolyte s with each of the positively charged (with valence $\upsilon_s^+ = 1$) or the negatively charged ion ($\upsilon_s^- = -1$) is a monomer that fits a lattice site. In this calculation, the solvent (water) is also modeled as a monomer. The acid groups A exist in two possible states, either charged $\upsilon_{A^-} = -1$ or in a neutral form $\upsilon_{HA} = 0$. The water molecules have three distinct states; most of it is in the neutral form $\upsilon_{H_2O} = 0$, whereas the other states are $\upsilon_{H_3O^+} = 1$ and $\upsilon_{OH^-} = -1$. The concentration of each states depends on the pH with corresponding $pK_w = 14$. The dissociation constant of the polyacid group pK_a is set to 4.25, which is the value for a carboxylic group.[35]

Besides the electrostatics, which is accounted for on the Poisson−Boltzmann level, we have short-range nearest-neighbor interactions parametrized by well-known Flory Huggins parameters. The chosen values are consistent with water being a selective solvent, i.e., $\chi_{AB} = \chi_{Bs} = 1.6$, where s is the electrolyte monomer, and $\chi_{BW} = 1.3$, which indicates strong repulsion between these segments. An athermal interaction parameter between the polyacid group and water is used ($\chi_{AW} = 0$), which reflects its hydrophilicity (miscibility with solvent).

The basis for computing the partition function of inhomogeneous polymer systems is the Edwards diffusion equation, where polymer segments experience a segment-type potential field dependence.[36] Within this scheme, chain conformations are effectively generated using a first-order Markov approximation, in which the degeneracy ω_c of each conformation (specified sequence of visited coordinates r_s^c by the segments $s = 1, ..., N$ of the chain in conformation c) is computed using the step probabilities mentioned above. As the r coordinates of all segments s are known, the overall potential u_c of a given conformation c is available, i.e., $u_c = \sum_s u(r_s^c)$. The number of chain in this conformation is given by $n_c = C\omega_c e^{-u_c/k_BT}$, where C is a normalization constant chosen such that the total number of molecules in the system is according to the specifications (input value) and k_BT is the thermal energy. Once all conformations are summed up, one has excess to all volume fraction profiles $\varphi_X(r)$ where $X = A, B, s, W$, including all possible internal states of A and W. We use the multiple-state approach of Bjorling et al.[37] to properly account for the internal state equilibria.

The self-consistent potentials follow the volume fractions profiles. In particular, we account for the short-range interactions using the Flory−Huggins parameters and Coulombic interactions. For the latter we have implemented the discrete form of the Poisson equation, in which for the case of spherical coordinate system

$$\epsilon_0 \frac{1}{r^2} \frac{d}{dr}\left(r^2 \epsilon_r(r) \frac{d\Psi(r)}{dr}\right) = -\rho(r), \forall r \in [0, M] \qquad (28)$$

where the local relative dielectric constant $\epsilon_r(r)$ are found by a volume fraction weighted average of segmental relative dielectric permittivities. The local charge distribution $\rho(r)$ are found in similar way, i.e., $\rho(r)/e = \sum_X \sum_j \upsilon_{X_j}(r)\varphi_{X_j}(r)$, where e is the

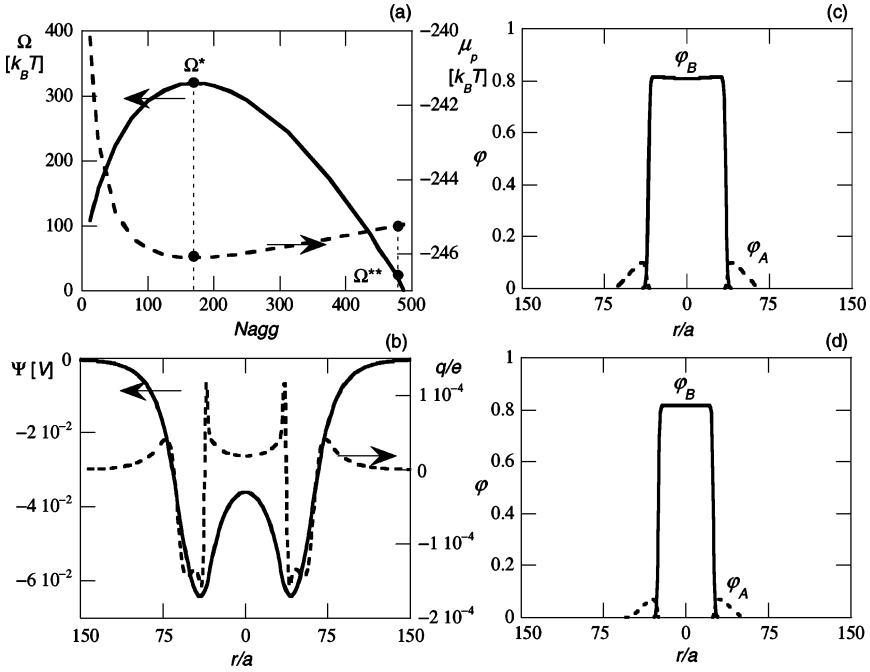

Figure 2. (a) Plot of the grand potential Ω and chemical potential of copolymers μ_p as a function of aggregation number N_{agg}. The first set of dots at $N_{agg} \approx 175$ indicates the theoretical cmc, i.e., the first appearance of thermodynamically stable micelles. It is indicated by Ω* on the Ω curve. The second set of dots at $N_{agg} \approx 480$ corresponds to the grand potential value $\Omega^{**} = 10k_BT$. This system is taken to depict the electrostatic potential Ψ and charge density q in (b) and the radial volume fraction φ of block copolymers A and B in (c). The profiles φ_A and φ_B at theoretical cmc is depicted in (d). The radial coordinate is denoted as r. All the plots are for the block copolymer $A_{100}B_{300}$ at pH = 3 and $\varphi_s = 10^{-5}$.

elementary charge, $\upsilon_{X_j}(r)$ is the total number of charges (per unit area) of segment X at the possible state j in layer r, and $\varphi_{X_j}(r)$ is the corresponding volume fraction which is subjected to the incompressibility constraint $\sum_X \sum_j \varphi_{X_j}(r) = 1$ for all coordinates r. By solving this Poisson eq 28, one obtains the local electrostatic potential $\Psi(r)$. For water we choose the relative dielectric constant to be 80. For all other components we choose a lower value of $\epsilon_r = 10$. Besides short-range and electrostatic interactions, in the segment potential field there is also a segment polarization term as well as a Lagrange contribution.[38]

In summary, for each segment type there are two conjugated distribution, i.e., the radial volume fraction profile $\varphi_X(r)$ and the radial potential profile $u_X(r)$, which should be consistent with each other. Typically, the number of copolymer molecules in the system is an input parameter as well as the pH and the electrolyte volume fraction in the bulk solution (semi-open ensemble). In equilibrium with the micellar object at the center of the coordinate system, there are few copolymer chains exist as unimers in the bulk solution. The volume fraction of one of the electrolyte ions is used to impose the electroneutrality condition in the bulk. Once all potentials and volume fractions are known, the grand potential Ω is evaluated as follows[39]

$$\frac{\Omega}{k_BT} = -\sum_r L(r)\,\Pi(r) \tag{29}$$

where $-\Pi(r)$ is the dimensionless grand potential density

$$\Pi(r) = \sum_X \sum_j \varphi_{X_j}(r)\frac{u_{X_j}(r)}{k_BT} + \sum_i \frac{\varphi_i(r) - \varphi_i^b}{N_i} - \frac{1}{2}\sum_X \sum_j \sum_Y \sum_k \chi_{X_jY_k}\{\varphi_{X_j}(r)(\langle\varphi_{Y_k}(r)\rangle - \varphi_{Y_k}^b) - \varphi_{X_j}^b(\varphi_{Y_k}(r) - \varphi_{Y_k}^b)\} - \frac{1}{2}\sum_X \sum_j e\upsilon_{X_j}\varphi_{X_j}(r)\frac{\Psi(r)}{k_BT} \tag{30}$$

In eq 30, the radial potentials of segment X at state j is denoted by $u_{X_j}(r)$ and $\varphi_i(r) = \sum_s \varphi_i(r,s)$, i.e., sum of the volume fraction of all segments of molecule i in layer r, whereas $\varphi_i(r,s)$ are obtained from the statistical weight of the segments in molecule i (known as segment-weighting factors); N_i is the total number of segments of molecule i. Furthermore, the superscript b denotes the variables in the bulk solution, and the angular bracket indicates that the volume fraction is averaged over neighboring layers (nonlocal Bragg−Williams approximation). The last term of eq 30 is the electrostatic contribution, where e is the elementary charge and υ_{X_j} is the valence of segment X at state j.

IV. Results and Discussion

From the calculations, various equilibrium structural properties of spherical micelles such as the size and aggregation number, as well as corresponding thermodynamic quantities, are obtained. We start with a small subsection presenting a case study. This allows us to elaborate on the way SCF results are coupled to the thermodynamics of small systems. The case study is followed by the analysis of the properties of the micelles as a function of pH and salt volume fraction φ_s. In the last subsection, the coexistence of different micellar sizes in a narrow pH range and low φ_s value is analyzed in more detail.

A. Case Study: $A_{100}B_{300}$, pH = 3, $\varphi_s = 10^{-5}$. This subsection is started with the discussions of some properties of a micellar solution of the copolymer $A_{100}B_{300}$ at pH = 3 and $\varphi_s = 10^{-5}$. Under this condition, the micelles are very weakly charged, and just one type of micellar size exists, i.e., the crew-cut micelle. For this system, we present the grand potential and chemical potential of the copolymer as a function of the aggregation number and selected radial charge, electrostatic potential, and a few density profiles.

Figure 2a shows the plot of the grand potential Ω and the chemical potential of copolymers μ_p as a function of the aggregation number N_{agg}. Here, the stability constraint in eq 10

is satisfied beyond $N_{agg} \approx 175$. This value corresponds to the theoretical cmc where the grand potential value is large, i.e., at $\Omega^* \approx 325k_BT$. The theoretical cmc is defined as the bulk concentration of polymer where stable micelles start to form, i.e., where $\partial\Omega/\partial N_{agg} = 0$. At the theoretical cmc, the chemical potential of copolymers is the lowest and gradually increasing with aggregation number. As $\Omega^* \approx 325k_BT$, the micellar volume fraction $\varphi_m \simeq e^{-\Omega^*/k_BT}$ is extremely small. Experimentally, it is impossible to observe such a low concentration of micelles. With increasing polymer concentration, the volume fraction of micelles increases as Ω decreases and N_{agg} increases dramatically. Quite arbitrary, the grand potential value $\Omega^{**} = 10k_BT$ is chosen as a point of reference for an experimentally accessible micelle. This value is chosen differently from the zero grand potential that is used by Borisov and Zhulina in their analysis.[5,6] It is clear however that both approaches lead to the same trends. Our Ansatz is internally consistent since it is assumed in the model that the micelles exist in the dilute regime. A value of grand potential $\Omega = 10k_BT$ is used to ensure a sufficient amount of translational entropy.

In Figure 2b, the radial profiles of the electrostatic potential $\Psi(r)$ and charge density $q(r)$ are plotted for the micelle with $N_{agg} \approx 480$. The small negative charge in the corona is due to the presence of the deprotonated polyacid segments which are locally compensated by excess small counterions. Figure 2b shows that the charge relaxes to zero in the bulk according to the classical description of the electric double layer. Because of the electroneutrality, the integrated charge density q in the whole system is equal to zero. In the region where most of the hydrophobic groups are found (core of the micelle), the dielectric permittivity is low, and this micellar part remains virtually free of charges (positive charge exists due to the presence of counterions at the core−corona region). The corona region, where most of the polyacid block can be found, is negatively charged, and an excess of counterions is accumulated in the core−corona and corona−solution interfaces. The charge distribution inside and around the micelle induces an electrostatic potential $\Psi(r)$, which in this case is negative throughout the system. The maximum electrostatic potential is found in the corona, and it vanishes in the bulk. Inside the core, the potential remains finite.

The radial profiles of volume fraction φ_A and φ_B are shown in parts c and d of Figure 2, corresponding to the micelle at Ω^{**} and Ω^*, respectively. For these micelles, the core and corona are easily located since the densely packed hydrophobic B and hydrated hydrophilic A blocks are spatially well separated. The profiles in both figures have very similar characteristics, and the change in N_{agg} is mostly reflected in the change of the core size. Throughout the article, the thickness of the corona T_{corona} of a micelle is computed as the first moment of the volume fraction of A groups with respect to the center of the micelle ($r = 0$) minus the core radius R_{core}, which is obtained directly from the density profile φ_B (R_{core} is twice the first moment of φ_B). The micelle at Ω^{**} ($T_{corona} = 11.94$, $R_{core} = 34.94$) is significantly larger than the micelle at Ω^* ($T_{corona} = 10.81$, $R_{core} = 24.61$). All sizes are in the units of lattice size a.

B. Ionic Strength and pH Dependences. In the following, unless indicated otherwise, all of the results are for micelles with a grand potential equal to $\Omega = 10k_BT$. The corresponding micelles, with micellar volume fraction $\varphi_m = e^{-10} \approx 4.5 \times 10^{-5}$, are considered to be the ones which are found near the experimental cmc.

In Figure 3, two set of plots of aggregation number N_{agg} as a function of pH are shown. Figure 3a shows monotonically

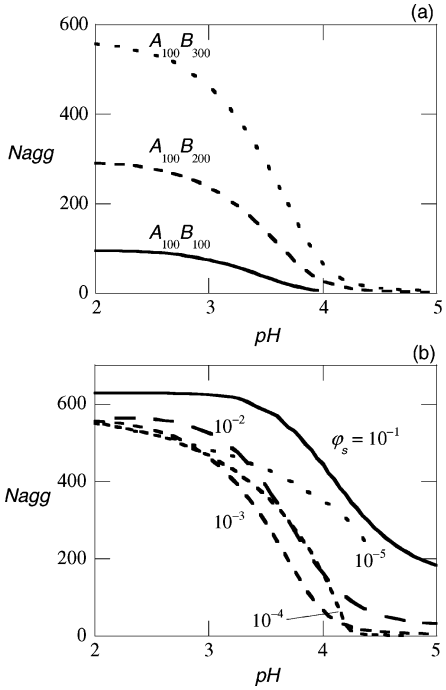

Figure 3. (a) Plot of the aggregation number N_{agg} as a function of pH at a restricted grand potential $\Omega = 10k_BT$ and $\varphi_s = 10^{-3}$ for different block copolymers as indicated: $A_{100}B_{100}$, $A_{100}B_{200}$, and $A_{100}B_{300}$. (b) A similar plot for block copolymer $A_{100}B_{300}$ at the same Ω value for different electrolyte volume fraction φ_s as indicated.

decreasing N_{agg} as pH increases for the copolymers $A_{100}B_{100}$, $A_{100}B_{200}$, and $A_{100}B_{300}$ at $\varphi_s = 10^{-3}$. At a fixed pH, the aggregation number increases with the length of the hydrophobic tail B due to a stronger hydrophobic attraction for longer tail moiety. For each copolymer, the N_{agg} decreases with pH, and this decrease is more pronounced for longer tail lengths. As the pH increases, the number of charges in the polyacid block increases. This increase in degree of dissociation α_{A^-} leads to a more repulsion between the headgroup segments. This explains the decrease of the aggregation number. A complementary explanation for the decrease of the aggregation number N_{agg} with increasing pH is that the proton charge is, to a first order, locally compensated by the accumulation of counterions. The local increase in the osmotic pressure promotes the hydration of the corona such that the corona occupies more space. Geometric considerations predict a decrease of the aggregation number.

Figure 3b shows a significantly more complex behavior of N_{agg} as a function of pH for a wide range of φ_s. For each value of φ_s, N_{agg} is a monotonically decreasing function of pH because of the accumulation of charges in and around the corona. Interestingly, some of the curves for different φ_s values cross each other. This indicates a nonmonotonic behavior of the aggregation number with increasing electrolyte concentration φ_s (at a given pH). In the range of φ_s from 10^{-3} to 10^{-1}, the aggregation number drops at low pH, and in the range of φ_s from 10^{-3} to 10^{-5}, the aggregation number drops at high pH. This nonmonotonic behavior can be seen more clearly in Figure 4. Here, N_{agg} is depicted as a function of φ_s for three different pH values. At pH = 2, the aggregation number varies hardly with φ_s since the polyacid block is uncharged. For pH = 4, the N_{agg} decreases from around 350 at $\varphi_s = 10^{-5}$ to around 50 at $\varphi_s = 10^{-3}$ and rebounds to $N_{agg} \approx 400$ at $\varphi_s = 10^{-1}$. At pH = 5, only stable micelles are found for $\varphi_s > 10^{-3}$.

To understand better how N_{agg} is a function of pH and φ_s, let us discuss the degree of dissociation of the acid groups in

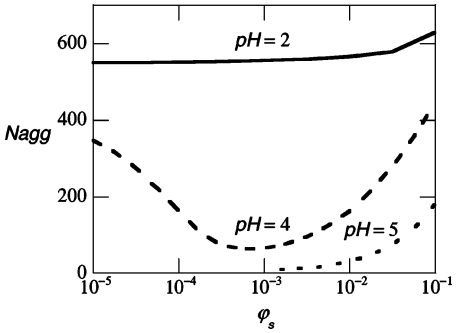

Figure 4. Plot of the aggregation number N_{agg} as a function of electrolyte concentration φ_s for a few pH values as indicated at the grand potential $\Omega = 10k_BT$ for block copolymer $A_{100}B_{300}$.

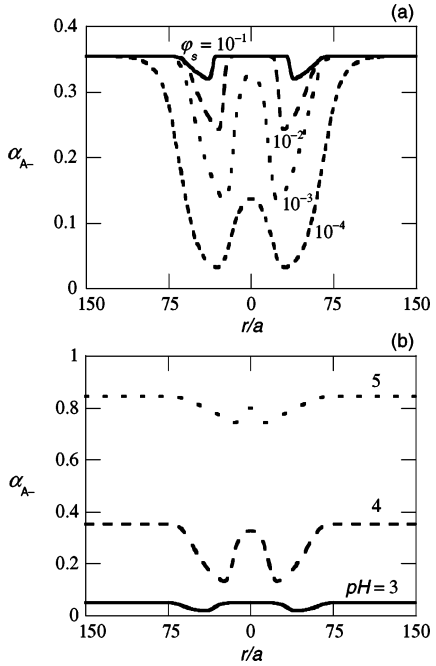

Figure 5. (a) Degree of dissociation α_{A^-} along radial direction r from the center of a micelle from the $A_{100}B_{300}$ block copolymers at pH = 4 and varying φ_s, as indicated. (b) A similar plot at salt concentration $\varphi_s = 10^{-3}$ at different pH.

the corona in more detail. For this purpose, the copolymer $A_{100}B_{300}$ is selected. In the annealed polyelectrolyte chain, the degree of dissociation α_{A^-} depends on the local pH and on the electrostatic potential, which is influenced by the presence of salt. In Figure 5, the profiles of the degree of dissociation α_{A^-} along the radial direction r from the center of a micelle are depicted for different electrolyte concentration φ_s and pH. In Figure 5a, the φ_s is varied from 10^{-1} to 10^{-4} at pH = 4, whereas in Figure 5b, the pH is varied from 3 to 5 for $\varphi_s = 10^{-3}$. As in Figure 3, N_{agg} is not fixed. In fact, the aggregation number decreases as pH increases (cf. Figure 3a), and for low φ_s, the aggregation number decreases as φ_s increases and the reverse is found for high φ_s (cf. Figure 3b). A close inspection of Figure 5 allows an estimation of the micellar size. It can be seen from Figure 5 that the core and corona sizes change correspondingly with N_{agg}.

In general, the degree of dissociation is suppressed by the negative electrostatic potential Ψ. Thus, the degree of dissociation of the headgroups A in the corona of the micelle is smaller than that in the bulk. However, it can be seen in Figure 5a that the degree of dissociation α_{A^-} remains relatively high in the corona region for a higher electrolyte concentration. Since the profile of α follows the electrostatic potential profile and since the electrostatic potential in the core is finite, the value of the degree of dissociation α_{A^-} in the core is significant. However, the contribution of this to the total charge in the micelle can be neglected due to the infinitesimal amount of polyacid in the core.

For varying pH (Figure 5b), the degree of dissociation outside the micelle follows the trend in the bulk; i.e., α_{A^-} increases with increasing pH. In the corona of the micelle, α_{A^-} is again suppressed due to the negative Ψ. When pH $\ll$ pK_a, the potential remains relatively low and the degree of dissociation α_{A^-} follows that in the bulk $\alpha^b_{A^-}$. When pH $\gg$ pK_a, α_{A^-} is only suppressed at sufficiently high Ψ. Again, α_{A^-} follows $\alpha^b_{A^-}$ to the first order. At intermediate pH, α_{A^-} is mostly suppressed in the micelle.

A similar nonmonotonic behavior for N_{agg} as a function of φ_s has been predicted analytically.[6] The cause of this nonmonotonic behavior is the opposite effect of the electrolyte on the charge characteristics in the micelle. By increasing electrolyte concentration, counterions screen the electrostatic repulsion between charged groups such that the effective charge diminishes and the electrostatic potential is reduced. The low Ψ leads to a generation of more charges by further dissociation. This increasing dissociation attracts more counterions and so forth. This cooperative effect of salt can develop best when pH $\approx$ pK_a. At more extreme pH values, the proton charge regulation is suppressed.

From the result such as in Figure 3a, it is found that aggregation number N_{agg} scales with the degree of polymerization m of hydrophobic group as $N_{agg} \sim m^x$ with $x = 1.6$ for crew-cut micelles and 1.8 for starlike micelles. The analytical prediction[6] for this proportionality is x between 1 and 2 for crew-cut micelles and 10/11 for starlike micelles.

The scaling of N_{agg} and other properties, such as R_{core} and T_{corona}, with φ_s depends strongly on the pH. As can be seen in Table 1, at low φ_s, $N_{agg} \sim \varphi_s^{-0.47}$ for crew-cut micelles at a pH close to the pK_a. At high φ_s, $N_{agg} \sim \varphi_s^y$ where y varies from 0.43 to 0.45 for crew-cut micelles and 0.7 to 0.9 for starlike micelles at a pH around the pK_a value. The scaling for the

Table 1. Analytical and Estimated Numerical SCF Values of Scaling Exponents of Micellar Properties R_{core}, T_{corona}, and N_{agg} from Block Copolymers A_mB_n in the Specified Physicochemical Conditions; Crew-Cut and Starlike Micelles Are Denoted by CC and SL, Respectively

	analytical		SCF	
	x	conditions	x	conditions
$R_{core} \sim \varphi_s^x$	−2	CC, low φ_s	−0.15	CC, pH ≈ pK_a, low φ_s
	0.4	CC, high φ_s	0.14 to 0.15	CC, pH ≈ pK_a, high φ_s
			0.24 to 0.3	SL, high pH and φ_s
$T_{corona} \sim \varphi_s^x$	1	CC, low φ_s	0.04 to 0.05	CC, pH ≈ pK_a, low φ_s
	−0.2	CC, high φ_s	−0.03	CC, pH ≈ pK_a, high φ_s
	−0.09	SL, high φ_s	−0.02 to −0.08	SL, high pH and φ_s
$N_{agg} \sim \varphi_s^x$	−6	CC, low φ_s	−0.47	CC, pH ≈ pK_a, low φ_s
	1.2	CC, high φ_s	0.43 to 0.45	CC, pH ≈ pK_a, high φ_s
	0.54	SL, high φ_s	0.7 to 0.9	SL, high pH and φ_s

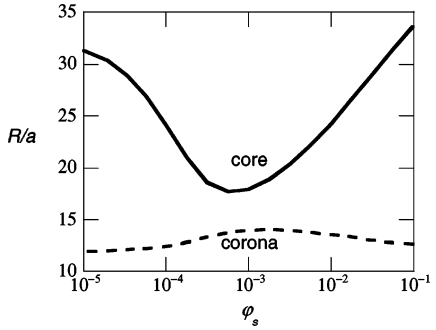

Figure 6. Radius of core and corona thickness of a micelle composed of $A_{100}B_{300}$ block copolymers as a function of salt volume fraction φ_s at pH = 4 and the grand potential $\Omega = 10k_BT$.

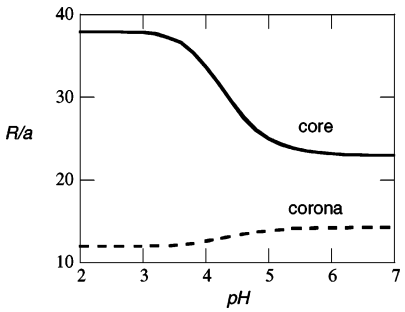

Figure 7. Radius of the core and corona thickness of a micelle from $A_{100}B_{300}$ block copolymers as a function of pH at $\varphi_s = 10^{-1}$. The restricted grand potential Ω is equal to $10k_BT$. All micelles are in the crew-cut form.

aggregation number of starlike micelles is close to the analytical prediction by Zhulina and Borisov, which is $N_{agg} \sim \varphi_s^{6/11}$. However, for the case of crew-cut micelles, the scaling is considerably less than the prediction of Zhulina et al.,[6] which is $N_{agg} \sim \varphi_s^{-6}$ for low φ_s and $N_{agg} \sim \varphi_s^{6/5}$ for high φ_s.

Corresponding to the change in the aggregation number as a function of the electrolyte concentration φ_s, the core and corona sizes change nonmonotonically as can be seen in Figure 6. The parameter R represents either the radius of the core R_{core} or corona thickness T_{corona} in units of the length of a lattice site a. The $A_{100}B_{300}$ copolymer is selected for fixed pH = 4. The core size follows the dramatic change of N_{agg}. However, the corona thickness changes less severely than the core radius. The corona of the micelle, which mostly consists of polyacid block A, undergoes two opposite effects. The change of N_{agg} should lead to a similar change of T_{corona}. However, the variation in N_{agg} is driven by the increase (for $\varphi_s < 10^{-3}$) or decrease (for $\varphi_s > 10^{-3}$) of repulsion between the polyelectrolyte groups in the corona. These electrostatic effects cause the hydrophilic chains to stretch for $\varphi_s < 10^{-3}$ or to contract for $\varphi_s > 10^{-3}$, compensating the trend of the core. These two opposite effects lead to a relatively weak dependence of T_{corona} with φ_s.

Similar compensating effects are seen in Figure 7. Here, the core radius and corona thickness of the micelle formed from $A_{100}B_{300}$ are depicted as a function of pH at fixed $\varphi_s = 10^{-1}$. The core radius follows the aggregation number (Figure 3b); i.e., R_{core} decreases at increasing pH. The corona thickness increases steadily until it reaches an asymptotic value at pH > 5. Beyond pH = 5, the micellar properties become a weak function of pH since the polyelectrolyte groups in the corona are fully charged. In both Figures 6 and 7, there is no intersection between core and corona curves. This means that in these systems only crew-cut micelles exist.

More insight into the structural properties of crew-cut micelles is obtained from radial density profiles. Radial profiles of the

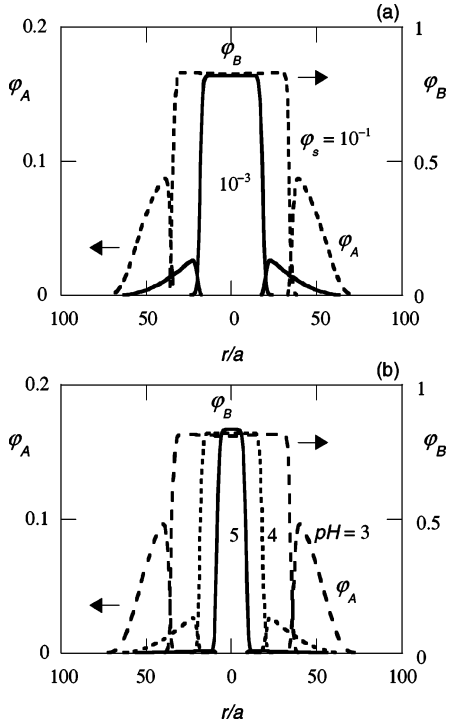

Figure 8. (a) Profiles of the volume fraction φ of A and B groups of block copolymers in a spherical micelle along the radial direction r through the center of the micelle which is located at the point of origin. The micelle is composed of $A_{100}B_{300}$ block copolymers at pH = 4 and salt volume fraction $\varphi_s = 10^{-1}$ and 10^{-3}. (b) Similar profile for pH = 3, 4, and 5 as indicated at fixed $\varphi_s = 10^{-3}$. The radial density φ_A for pH = 5 is extremely small such that it is difficult to see the profile in this coordinate scale. As in the case study, all of the volume fraction φ_B in the core reach the value of ≈0.8.

volume fraction φ of A and B groups of copolymer in a micelle are shown in Figure 8. Here, the center of the micelle is located at $r = 0$, and the micelle is composed of $A_{100}B_{300}$ block copolymers. Radial profiles of micelles at pH = 4 for a set of electrolyte concentrations are presented in Figure 8a. Profiles of micelles at $\varphi_s = 10^{-3}$ for a few pH values are depicted in Figure 8b. In this figure, the core of the micelle is easily identified by the homogeneous density of the hydrophobic group B. The polyacid group A is accumulated in the corona region. As already described before, it can be seen that the R_{core} increases and T_{corona} decreases slightly for higher φ_s (see Figure 6 for the overall size changing). By increasing pH, the opposite happens, the R_{core} decreases and T_{corona} increases, such that eventually the starlike micelles are formed. It should be noted that due to the application of a monomeric solvent in the model, the volume fraction of hydrophobic group φ_B in the core is not equal to unity. In fact, it reaches a constant value of ≈0.8 (cf. Figure 2c,d). The volume fraction of hydrophilic polyacid group φ_A depends strongly on φ_s and pH. High φ_s and low pH values lead to a higher local density of hydrophilic A groups in the corona. The radial density φ_A becomes extremely low at low φ_s and high pH. A large number of charges in the corona cause a more stretched chain in the corona which suppresses the core size and reduces N_{agg}. These effects lead to a very low density of segment A in the corona as can be seen for example at pH = 5 in Figure 8b. This can also be found later in Figure 10c where the same copolymer is used at slightly higher pH = 4.5 and lower electrolyte volume fraction $\varphi_s = 10^{-5}$. Further discussions about the presence of the starlike micelles and the transition between crew-cut and starlike micelles can be found in the next section.

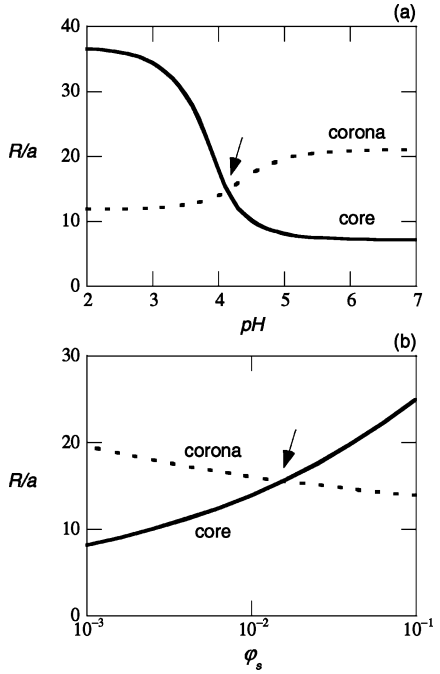

Figure 9. (a) Radius of the core and the corona thickness of micelles composed of $A_{100}B_{300}$ block copolymers as a function of the pH at $\varphi_s = 10^{-3}$. (b) Similar plot for varying salt volume fraction φ_s at pH = 5. For both figures, the grand potential $\Omega = 10k_BT$. The arrows indicate the transition point.

As can be seen in Table 1, the core radius scales with the electrolyte volume fraction as $R_{core} \sim \varphi_s^x$. For the case of crew-cut micelles, x is equal to -0.15 at low φ_s and 0.14 at high φ_s for pH close to the pK_a. For starlike micelles, x varies from 0.24 to 0.3 at high φ_s. The scaling of the corona thickness T_{corona} with the electrolyte concentration $T_{corona} \sim \varphi_s^y$ gives for the case of crew-cut micelles; y is about 0.04 at low φ_s and -0.03 at high φ_s for a pH close to the pK_a. For starlike micelles, y is around -0.08. The analytical prediction of the scaling of the size with φ_s are $R_{core} \sim \varphi_s^{-2}$ at low φ_s and $\sim\varphi_s^{2/5}$ at high φ_s for crew-cut micelles.[6] The thickness of corona scales as $T_{corona} \sim \varphi_s$ at low φ_s and $\sim\varphi_s^{-1/5}$ at high φ_s for crew-cut micelles and $T_{corona} \sim \varphi_s^{-1/11}$ for starlike micelles.

A large discrepancy between analytical and numerical calculation happens for the case of crew-cut micelle. Possible explanations for this discrepancy are that in the numerical work the polyelectrolyte group does not contain enough charges at pH < pK_a or that the hydrophilic and hydrophobic lengths m and n are not large enough to find the limiting scale. It should be noted that the box profile used in the analytical work is a severe approximation, especially for a spherical coordinate system, so that it is not surprising that the scaling predictions are not exactly reproduced.

C. Transition between Crew-Cut and Starlike Micelles. Until now, we have discussed the case when the core radius is larger than the corona thickness. When φ_s in the system is lowered, the opposite is found. A smooth transition between crew-cut (CC) and starlike (SL) micelle occurs as pH or φ_s changes. This transition, for example, can be seen in Figure 9. Here, the size of the micelle that consists of copolymers $A_{100}B_{300}$ at $\varphi_s = 10^{-3}$ changes with pH (Figure 9a) and at pH = 5 varies with φ_s (Figure 9b). In Figure 9a, as the pH increases, the core radius decreases, and the thickness of corona increases smoothly. When the pH value is close to pK_a, $R_{core} = T_{corona}$ (as indicated by the arrow). For pH < pK_a, the micelles are in the crew-cut form, and for pH > pK_a, starlike micelles are found. The reverse is found for increasing φ_s at fixed pH as can be seen in Figure 9b. Beyond $\varphi_s \approx 1.5 \times 10^{-2}$, where the core and corona size are equal, crew-cut micelles are found, and at low φ_s starlike micelles exist.

It is important to note that this transition only happens at sufficiently high pH and relatively low φ_s values. The reason for this is that at high pH the copolymers, and consequently the micelles, are highly charged such that the headgroup is more responsive to the change of added electrolyte concentration. At low φ_s, the polyacid block in the headgroup is unscreened and the degree of dissociation α_{A^-} is low. The micellar structure changes rapidly when the total charge in the corona increases with pH. To illustrate this, we refer again to the radial density profiles of the micelles for various pH values given in Figure 8b. At pH = 3 crew-cut micelles prevail, whereas at pH = 5 starlike micelles are found.

Clearly, upon changes in φ_s or pH, a smooth transition between crew-cut and starlike micelles occurs at $\varphi_s \approx 10^{-3}$. Remarkably, these two micellar forms also coexist in a particular range of pH and φ_s values. This occurs at even lower φ_s. The best way to show the coexistence between these two micellar size is by considering the corresponding restricted grand potential Ω. To find two different micellar sizes that coexist, there must be two regions of Ω that meet the stability condition which is given in eq 10. Moreover, the chemical potential of the copolymers should be identical for these two cases. An example of this is shown in Figure 10 for copolymer $A_{100}B_{300}$ at pH = 4.5 and $\varphi_s = 10^{-5}$. In Figure 10a, it is shown that the grand potential curve has a negative slope at $N_{agg} < 7$ and at $N_{agg} > 85$. In Figure 10b, the corresponding μ_p is plotted. Since $\partial\Omega/\partial\mu_p = -N_{agg}$, the stable micellar region is where the slope of the μ_p curve is positive (eq 26). In this case, it occurs at $N_{agg} < 7$ and at $N_{agg} > 85$. In these two regions, thermodynamically stable micelles are found, whereas in the intermediate range, $7 < N_{agg} < 85$, the slope is positive, representing unstable micellar structures. Moreover, the first stable region corresponds to small starlike micelles, and the second stable region corresponds to large crew-cut micelles. The radial profiles of the volume fractions φ_A and φ_B of the two coexisting micelles at corresponding positions 1 and 2 (as indicated in Figure 10a) can be seen in parts c and d of Figure 10 for starlike and crew-cut micelles, respectively. These micelles exist at the selected value of the chemical potential $\mu_p' \approx -249.5k_BT$ (cf. Figure 10b). For the starlike micelle, $R_{core} = 6.34$ and $T_{corona} = 15.64$; for the crew-cut micelle, $R_{core} = 24.74$ and $T_{corona} = 10.86$ (in the units a).

The local radial density of the polyelectrolyte segment A in the corona for the starlike micelle is much lower than that for the crew-cut micelle (note the difference in scales between parts c and d of Figure 10). In Figure 10c, the noticeable overlap between the radial densities of φ_A and φ_B in the core−corona interface is due to the low segment density φ_A. As already mentioned before, the radial density φ_A becomes extremely low at low φ_s and high pH. This is due to the large number of charges present in the corona that leads to strongly stretched and radially extended polyelectrolyte chains.

The chemical potential μ_p of the copolymer as a function of N_{agg} is presented in Figure 10b. The horizontal line indicates where crew-cut and starlike micelles coexist. It can be seen that there is only a narrow region in which this coexistence can occur. It is governed by the narrow μ_p region where stable large crew-cut micelles can exist.

By applying eq 21 in the coexistence region, one can evaluate the concentration of copolymers that assemble into starlike and

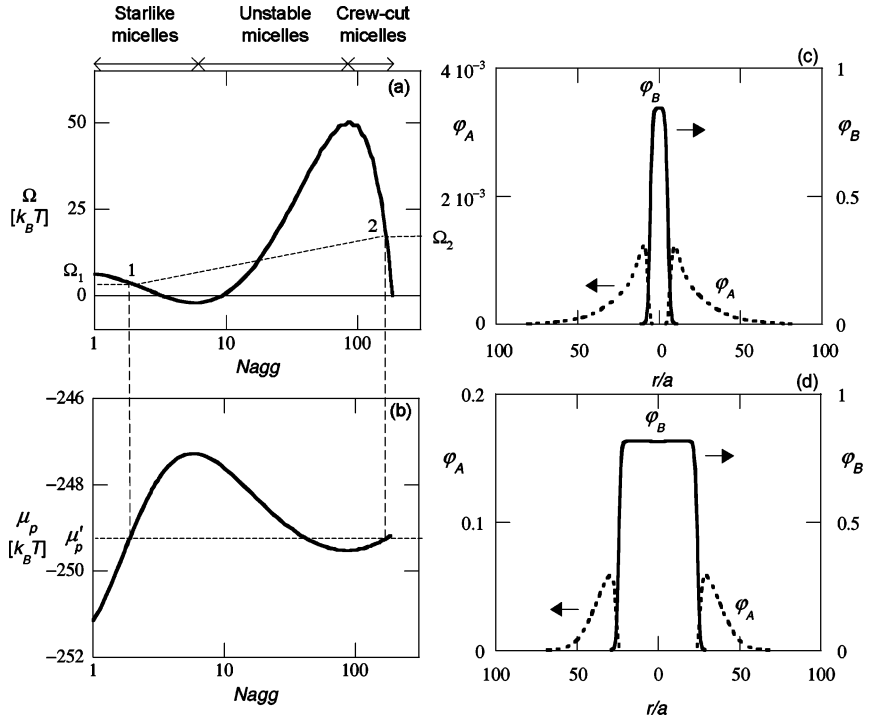

Figure 10. (a) Grand potential Ω as a function of aggregation number N_{agg} (in logarithmic scale). Regions with negative slope indicates the existence of stable micelles. The diagonal dashed line corresponds to an example of two micelles that coexist at the same chemical potential μ_p'. They are indicated as 1 and 2. (b) Copolymer chemical potential μ_p as a function of aggregation number N_{agg}. The horizontal line represents two coexisting stable micelles. The micelles are composed of block copolymers $A_{100}B_{300}$ at pH = 4.5 and $\varphi_s = 10^{-5}$. (c) Radial profiles of the volume fractions φ_A and φ_B of the micelle at 1 as indicated in (a). (d) Radial profiles of the volume fractions φ_A and φ_B of the micelle at 2 as indicated in (a). In (c) and (d), φ_B is shown by a solid line and φ_A by a dashed line. In both (c) and (d), φ_B reaches the value at about 0.8 in the core region (outside the scale) as in Figure 8.

crew-cut micelles. The contributions to the total copolymer concentration are depicted in Figure 11. In Figure 11a, the volume fraction of copolymers in the bulk, both in small and in large micelles, are plotted as a function of the bulk value φ_p^b. In Figure 11b, the total volume fraction of copolymers φ_p is plotted at different bulk values. It can be seen that as the copolymer concentration increases beyond the cmc, small micelles are initially formed. It is then followed by the coexistence between small and large micelles at higher φ_p. In this coexistence region, the relative contribution of the large micelles increases abruptly and becomes dominant over the small ones. Only in a very narrow region, as indicated with an arrow in Figure 11b, the amount of copolymers in the large and small micelles is of the same order.

The mole fractions of coexisting small and large micelles with increasing copolymer volume fractions φ_p are obtained using eq 19 and imposing volume conservation. The result is depicted in Figure 12. Here, X_1 is the mole fraction of the small starlike micelle and X_2 is that of the large crew-cut micelle. As the amount of copolymers increases, the crew-cut micelles appear and quickly dominate so that the relative contribution of starlike micelles diminishes. The number of small and large micelles are equal at $\varphi_p \approx 7 \times 10^{-2}$. Beyond this value, the large micelles are more dominant as already described above.

At low electrolyte volume fraction ($\varphi_s = 10^{-5}$), there is a narrow pH region of coexistence. This coexistence is manifested in various micellar properties as illustrated in Figure 13. In Figure 13a the N_{agg} is plotted as a function of pH, and in Figure 13b the bulk degree of dissociation of segment state A^- ($\alpha_{A^-}^b$) and the average degree of dissociation in the micelle $\langle\alpha_{A^-}\rangle$ are plotted. As previously described, N_{agg} decreases with increasing pH, but the intermediate N_{agg} values vanish and a narrow pH range is found for which two different values of N_{agg} coexist.

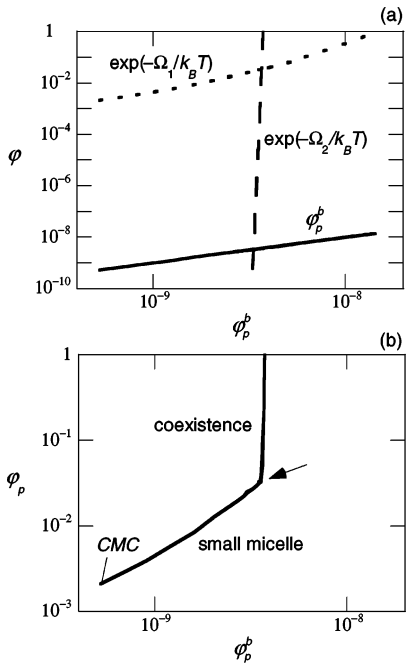

Figure 11. (a) Various contribution of the total block copolymer volume fraction φ_p as a function of its bulk value φ_p^b. small micelles $X_1\varphi_m = e^{-\Omega_1/k_BT}$, large micelles $X_2\varphi_m = e^{-\Omega_2/k_BT}$, and free copolymers in the bulk φ_p^b for copolymers $A_{100}B_{300}$ at pH = 4.5 and $\varphi_s = 10^{-5}$. (b) Total copolymer volume fraction φ_p as a function of φ_p^b. The starting point of the curve gives the total copolymer concentration at the cmc where the first stable micelles appear. The arrow denotes the region where the contribution to the total copolymer concentration of the large and small micelles is the same.

The average degree of dissociation of polyacid block $\langle\alpha_{A^-}\rangle$ increases with pH. As can be seen in Figure 13b, the average

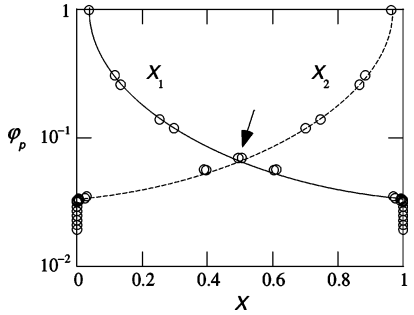

Figure 12. Total copolymer volume fraction φ_p with corresponding mole fraction of small micelles X_1 and big micelles X_2 in the micellar ensemble for copolymers $A_{100}B_{300}$ at pH = 4.5 and $\varphi_s = 10^{-5}$. The arrow indicates the point where $X_1 = X_2$ at $\varphi_p \approx 7 \times 10^{-2}$.

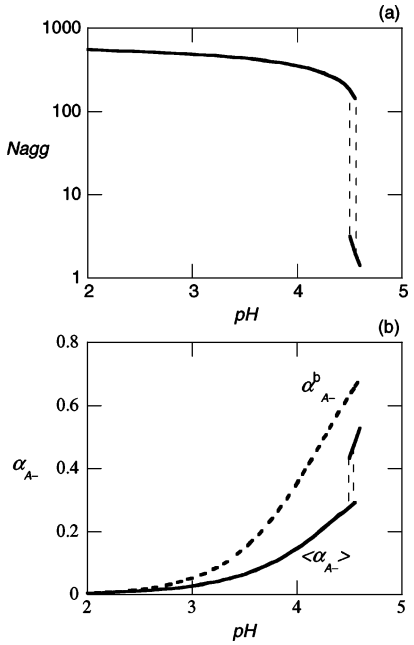

Figure 13. (a) Plot of the aggregation number N_{agg} vs pH at $\Omega = 0$ of micelles composed of block copolymers $A_{100}B_{300}$ at $\varphi_s = 10^{-5}$. The coexistence zone is in between the two dashed lines. (b) Plot of the degree of dissociation of the polyacid block in the bulk $\alpha^b_{A^-}$ and its average $\langle\alpha_{A^-}\rangle$ in the micelle.

degree of dissociation is less than that in the bulk. Analogous to N_{agg}, the intermediate $\langle\alpha_{A^-}\rangle$ values do not occur, and two different values of $\langle\alpha_{A^-}\rangle$ coexist in a narrow pH range. As indicated, the coexistence region is in between the two dashed lines, i.e., at 4.45 < pH < 4.55. At pH < 4.45, only crew-cut micelles exist, and at pH > 4.55, only starlike micelles are found. In the coexistence region, two micelles exist in different proportions, as already explained previously for the case of pH = 4.5 (cf. Figure 12).

Having demonstrated the presence of a coexistence region of crew-cut and starlike micelles on thermodynamic grounds (as discussed extensively above), we proceed to show the evolution of a thermodynamic property, such as Ω, for varying pH and φ_s. A selected set of results is shown in Figure 14, both for the case of varying pH at fixed electrolyte volume fraction $\varphi_s = 10^{-5}$ (Figure 14a) and for varying φ_s at fixed pH = 4.5 (Figure 14b). Again, the region where the value of Ω is negative is considered experimentally inaccessible. Moreover, stable micelles exist in the region where the slope $\Omega(N_{agg})$ is negative. In Figure 14a, it can be seen that up to pH = 4.35 there is only a single stable micellar region. At pH = 4.45, two stable micellar regions are found. In Figure 14b, at $\varphi_s = 10^{-1}-10^{-4}$, one stable

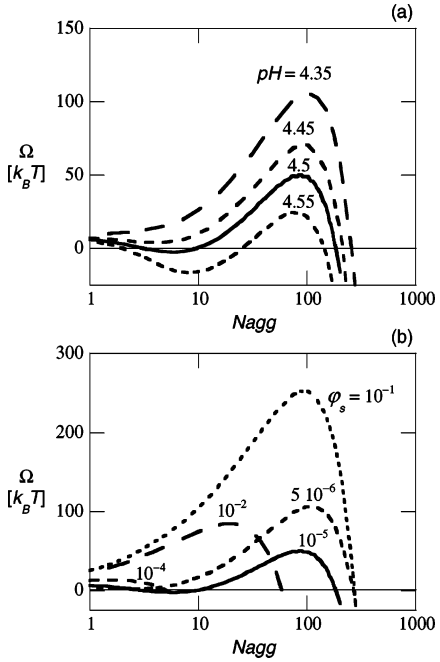

Figure 14. (a) Plot of the grand potential Ω as a function of the aggregation number in logarithmic scale at different pH values, as indicated. The block copolymer $A_{100}B_{300}$ is used, and the electrolyte volume fraction φ_s is fixed at 10^{-5}. (b) Similar plot for varying φ_s at fixed pH = 4.5.

micellar region exists. For $\varphi_s < 10^{-4}$, two stable regions appear. Note that the maximum value of the grand potential Ω_{max} first decreases with the decreasing φ_s, but for $\varphi_s < 10^{-4}$, Ω_{max} increases with decreasing φ_s. This increasing Ω_{max} for decreasing φ_s is another manifestation of the nonmonotonic behavior of micellar properties with respect to φ_s. As φ_s decreases, the peak moves first to a lower N_{agg} value and then it shifts again to a higher value (a similar example is already discussed in Figure 4).

From such sets of curves, one can locate the stable micellar regions for various pH or φ_s. As an example, the compilation of these regions in the pH vs N_{agg} system is depicted in Figure 15a. In this figure, the stable regions of starlike and crew-cut micelles are hatched and denoted as SL and CC, respectively. The bold curve indicates the stability boundaries which are obtained either from the first or the second maximum value of grand potential curve, denoted as Ω_{max1} or Ω_{max2}, respectively. The bold dashed curve in Figure 15a is obtained from the maximum grand potential with negative values. The thin curves are obtained from the minimum grand potential Ω_{min} or zero grand potential for the case of a negative Ω_{min}. The region of pH in between the two horizontal lines ($4.4 \lesssim$ pH $\lesssim 4.6$) of Figure 15a demarcates the coexistence zone.

Phase coexistence of two systems of finite size is unusual and thus extremely interesting. It has been shown previously in Figure 11 that by gradually increasing φ^b_p, i.e., by increasing the chemical potential μ_p of the copolymers in the system, one may find changes in the population of both crew-cut and starlike micelles. As these two populations do not respond in the same way, it is possible to change the relative ratio X of these micelles in the system. As a consequence, one can imagine that the two species are present at about the same quantities. Another finite-size effect is that, upon increasing the chemical potential of the copolymers, both micellar species increase their aggregation number modestly yet noticeably (Figure 10b). Indeed, the coexistence of these two micellar species is only possible since there is a free energy barrier that makes intermediate micellar

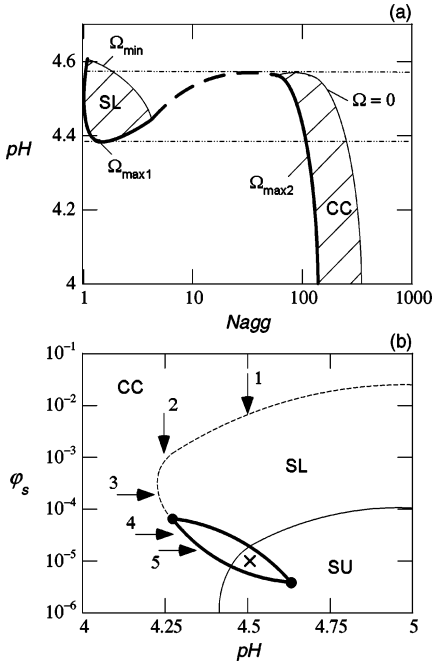

Figure 15. (a) Compilation of stable micellar regions in a pH vs N_{agg} diagram (shadowed) for the block copolymers $A_{100}B_{300}$ at $\varphi_s = 10^{-5}$. The stable starlike and crew-cut micelles are in the shadowed regions and denoted as SL and CC, respectively. The bold curves indicate the stability boundaries which are obtained from either the first or second maximum value of grand potential, denoted as Ω_{max1} or Ω_{max2}, respectively (cf. Figure 14). The bold dashed curve is obtained from the maximum of the grand potential which has negative value, while the thin curves are obtained either from the local minimum grand potential Ω_{min} or zero grand potential $\Omega = 0$. The region of pH in between the two horizontal lines demarcates the coexistence zone. (b) Microphase diagram of stable micellar regions for block copolymers $A_{100}B_{300}$. Crew-cut and starlike micelles are denoted as CC and SL, respectively. SU denotes the region where thermodynamically stable unimers are found. The coexistence exists in the region which is encapsulated by two bold curves. These curves composed of "spinodal points" for which crew-cut and starlike micelles coexist for the first time. The two curves intersect at two critical points which are indicated by two solid dots. The cross in the coexistence zone refers to the point which is plotted in Figures 10−12.

sizes thermodynamically unstable. This barrier is not infinitely high, and the finite size effects can systematically be investigated.

The micellar coexistence hints to a first-order-like phase transition that shows various analogies to first-order phase transitions in macroscopic systems. Within the terminology of first-order phase transitions, one should be able to identify a binodal and one or more spinodal conditions. At this stage, it is not completely clear which order parameter should be used to properly identify these quantities. In this respect, it is interesting to view the physicochemical conditions in terms of the pH and φ_s for which stable starlike micelles appear for the first time, while at the same chemical potential, the crew-cut micelles already exist. This should correspond to a type of spinodal point. Indeed, from Figure 15a, it is clear that one of such points on this curve is found for $\varphi_s = 10^{-5}$ at pH $\approx$ 4.4. A complementary point can be identified where the first crew-cut micelle is found when starlike micelles are already present. From Figure 15a, this point is at pH $\approx$ 4.6 for $\varphi_s = 10^{-5}$. These two "spinodal points" are transferred to a φ_s vs pH microphase diagram, as can be seen in Figure 15b. The complete set of spinodal points are indicated with two bold curves. These two curves intersect at two critical points which are indicated by solid dots. In this figure, the dashed line indicates the location of smooth transitions between crew-cut and starlike micelles. A region indicated as SU is located at high pH and low φ_s. In this region, already for $N_{agg} \approx 1$, unimeric micelles are thermodynamically stable. In this case, there is no gap between unimeric and micellar objects as true micellization does not occur. The fact that the thin curve that bounded the SU region intersects the coexistence zone indicates the possibility of coexistence between starlike micelles of unimeric size and large crew-cut micelles. An example of this has been discussed previously for the case of the copolymers $A_{100}B_{300}$ at $\varphi_s = 10^{-5}$ and pH = 4.5, as indicated by a cross in Figure 15b.

Following a path which is indicated by the arrow 1, the micelles change smoothly from the crew-cut (CC) to the starlike (SL) form at $\varphi_s \approx 5 \times 10^{-3}$. As φ_s is decreased further, the starlike micelles of unimeric size begin to be found, and at $\varphi_s \approx 2 \times 10^{-5}$ coexisting crew-cut micelles and starlike micelles of this type start to appear. Below $\varphi_s \approx 7 \times 10^{-6}$, again, only unimer-sized starlike micelles exist. A similar path, indicated by the second arrow at pH $\approx$ 4.25, gives the sequence CC−SL−CC upon decreasing φ_s, in which both transitions are smooth. The paths indicated by the third, fourth, and fifth arrows point to paths at fixed φ_s while pH is changed. In the third path, a smooth CC−SL transition is found, whereas the fourth path gives a stepwise change from CC to SL−SU through the coexistence region. A stepwise change from CC to SU through the coexistence region is expected following the fifth path.

In the analytical work by Zhulina and Borisov, the translational entropy as well as the mixing entropy of the various micelles was ignored. As argued before, the micelles with zero grand potential as selected by Zhulina and Borisov must always closely be related to the micelles with finite grand potential (we choose a typical value of $10k_BT$). As a result, the two approaches are comparable. In the analytical work, it is noted that the grand potential of the two type of micelles become zero for a fixed set of physicochemical conditions. From this, it was concluded that these micelles should coexist and that there is a first-order-like transition between these micellar entities. Our SCF analysis is more detailed, since nontrivial radial distributions are allowed, and the translational and mixing entropies are taken into account. Together with the SCF predictions, the analytical work may be used to select systems for experimental verification. This is very relevant since the coexistence only occurs in a narrow pH interval.

V. Conclusion and Remarks

Self-assembly of block copolymers that consist of a hydrophobic block and a hydrophilic annealed polyelectrolyte block is investigated by means of the self-consistent-field approximation. The hydrophobic (tail) block accumulates mainly in the core region of the micelles, and the polyelectrolyte headgroup is found in the strongly hydrated corona. As for the annealed polyacid segments, the degree of dissociation α_{A^-} increases with pH and electrolyte concentration φ_s. In our model, the long-range electrostatic interaction vanishes in the bulk solution, such that $\alpha^b_{A^-}$ is only governed by pH. The 1:1 electrolyte affects the degree of dissociation in the micellar region in a complex way.

The predicted nonmonotonic behavior of the equilibrium properties of the micelle,[5,6] such as the aggregation number N_{agg} and the micellar size, as a function of φ_s at fixed pH, is confirmed by the SCF computation. Salt ions have two counteracting effects: they screen the electrostatic potential in the corona and increase the degree of dissociation of this block. This antagonism leads to the nonmonotonic behavior of equilibrium properties. For crew-cut micelles, the numerical values

of scaling exponents of various micellar properties with φ_s are rather different from analytical predictions. This discrepancy may be caused by the limited total charge that is attained at low pH in which the crew-cut micelle is formed. The low degree of polymerization of the head and tail groups that is used for computational reasons may also contribute to this discrepancy. For starlike micelles, the scaling results from numerical calculation are quite close to the analytical predictions.

For high electrolyte concentration ($\varphi_s > 2 \times 10^{-2}$), only crew-cut micelles exist. As the pH increases, the charges in the corona remain fully screened such that the micellar characteristics do not change much. A smooth transition between crew-cut and starlike micelles is observed by increasing pH for $10^{-4} \lesssim \varphi_s \lesssim 10^{-2}$. The corona of the micelle is the more responsive upon increasing pH, the lower the φ_s (due to weaker screening effect). This is manifested in the significant change of corona size relative to the core size. At sufficiently low φ_s, there is a coexistence between crew-cut and starlike micelles in a narrow pH range. The first-order-like transition between these micellar types is analyzed in depth and is expected to be experimentally accessible.

Acknowledgment. The Dutch Science and Technology Foundation (STW), Aquacare, GWA, KIWA, Witteveen&Bos, and ETD&C are greatly acknowledged for financial support. Part of this work is supported by the Dutch National Science Foundation (NWO) program "Computational approaches for multi-scale modeling in self-organizing polymer and lipid systems", No. 047.016.004. The authors also acknowledge EU Polyamphi/Marie Curie program (FP6-2002, proposal 505027) and European Science Foundation EUROCORES Programme SONS-AMPHI (Project JA016-SONS-AMPHI).

References and Notes

(1) Wanka, G.; Hoffmann, H.; Ulbricht, W. *Colloid Polym. Sci.* **1990**, *268*, 101−117.
(2) Alexandridis, P.; Athanassiou, V.; Fukuda, S.; Hatton, T. A. *Langmuir* **1994**, *10*, 2604−2612.
(3) Monzen, M.; Kawakatsu, T.; Doi, M.; Hasegawa, R. *Comput. Theor. Polym. Sci.* **2000**, *10*, 275−280.
(4) Riess, G. *Prog. Polym. Sci.* **2003**, *28*, 1107−1170.
(5) Borisov, O. V.; Zhulina, E. B. *Macromolecules* **2002**, *35*, 4472−4480.
(6) Zhulina, E. B.; Borisov, O. V. *Macromolecules* **2002**, *35*, 9191−9203.
(7) Iatrou, H.; Willner, L.; Hadjichristidis, N.; Halperin, A.; Richter, D. *Macromolecules* **1996**, *29*, 581−591.
(8) Zhang, L.; Eisenberg, A. *Polym. Adv. Technol.* **1998**, *9*, 677−699.
(9) Heise, A.; Hedrick, J. L.; Frank, C. W.; Miller, R. D. *J. Am. Chem. Soc.* **1999**, *121*, 8647−8648.
(10) Burke, S.; Eisenberg, A. *High Perform. Polym.* **2000**, *12*, 535−542.
(11) Willner, L.; Poppe, A.; Allgaier, J.; Monkenbusch, M.; Lindner, P.; Richter, D. *Europhys. Lett.* **2000**, *51*, 628−634.
(12) Bosman, A. W.; Vestberg, R.; Heumann, A.; Frechet, J. M. J.; Hawker, C. J. *J. Am. Chem. Soc.* **2003**, *125*, 715−728.
(13) Laurati, M.; Stellbrink, J.; Lund, R.; Willner, L.; Richter, D.; Zaccarelli, E. *Phys. Rev. Lett.* **2005**, *94*, 195504.
(14) Currie, E. P. K.; Sieval, A. B.; Fleer, G. J.; Cohen Stuart, M. A. *Langmuir* **2000**, *16*, 8324−8333.
(15) Guo, X.; Ballauff, M. *Phys. Rev. E* **2001**, *64*, 051406.
(16) Scheutjens, J. M. H. M.; Fleer, G. J. *J. Phys. Chem.* **1979**, *83*, 1619−1635.
(17) Scheutjens, J. M. H. M.; Fleer, G. J. *J. Phys. Chem.* **1980**, *84*, 178−190.
(18) Hurter, P. N.; Scheutjens, J. M. H. M.; Hatton, T. A. *Macromolecules* **1993**, *26*, 5592−5601.
(19) Bohmer, M. R.; Evers, O. A.; Scheutjens, J. M. H. M. *Macromolecules* **1990**, *23*, 2288−2301.
(20) Bohmer, M. R.; Koopal, L. K. *Langmuir* **1992**, *8*, 1594−1602.
(21) Meijer, L. A.; Leermakers, F. A. M.; Nelson, A. *Langmuir* **1994**, *10*, 1199−1206.
(22) Meijer, L. A.; Leermakers, F. A. M.; Lyklema, J. *Pays Bas*. **1994**, *113*, 167−175.
(23) Meijer, L. A.; Leermakers, F. A. M.; Lyklema, J. *J. Phys. Chem.* **1995**, *99*, 17282−17293.
(24) Meijer, L. A.; Leermakers, F. A. M.; Lyklema, J. *J. Chem. Phys.* **1999**, *110*, 6560−6579.
(25) Claessens, M. M. A. E.; Van Oort, B. F.; Leermakers, F. A. M.; Hoekstra F. A.; Cohen Stuart, M. A. *Biophys. J.* **2004**, *87*, 3882−3893.
(26) Rabinovich, A. L.; Ripatti, P. O.; Balabaev, N. K.; Leermakers, F. A. M. *Phys. Rev. E* **2003**, *67*, 011909.
(27) Leermakers, F. A. M.; Rabinovich, A. L.; Balabaev, N. K. *Phys. Rev. E* **2003**, *67*, 011910.
(28) Israels, R.; Leermakers, F. A. M.; Fleer, G. J. *Macromolecules* **1994**, *27*, 3087−3093.
(29) Mercurieva, A. A.; Birshtein, T. M.; Zhulina, E. B.; Iakovlev, P.; van Male, J.; Leermakers, F. A. M. *Macromolecules* **2002**, *35*, 4739−4752.
(30) Hill, T. L. *Thermodynamics of Small Systems, Parts 1 and 2*; Dover Pub.: New York, 1994.
(31) Hall, D. G.; Pethica, B. A. In *Nonionic Surfactants*; Schick, M. J., Ed.; Marcel Dekker: New York, 1967; Chapter 16.
(32) Gibbs, J. W. *The Scientific Papers of J. Willard Gibbs*; Ox Bow Press: Woodbridge, 1993; Vol. 1.
(33) Leermakers, F. A. M.; Eriksson, J. C.; Lyklema, J. In *Fundamentals of Interface and Colloid Science V: Soft Colloids*; Lyklema, J., Ed.; Elsevier: Amsterdam, 2005; Chapter 4.
(34) Van der Schoot, P. P. A. M.; Leermakers, F. A. M. *Macromolecules* **1988**, *21*, 1876−1877.
(35) Van der Vegte, E. W.; Hadziioannou, G. *J. Phys. Chem. B* **1997**, *101*, 9563−9569.
(36) Edwards, S. F. *Proc. Phys. Soc., London* **1965**, *85*, 613−624.
(37) Bjorling, M.; Linse, P.; Karlstrom, G. *J. Phys. Chem.* **1990**, *94*, 471−481.
(38) Van Male, J. Self-Consistent-Field Theory for Chain Molecules: Extensions, Computational Aspects, and Applications, Doctoral Thesis, Wageningen, 2003.
(39) Evers, O. A.; Scheutjens, J. M. H. M.; Fleer, G. J. *Macromolecules* **1990**, *23*, 5221−5233.

MA060163T